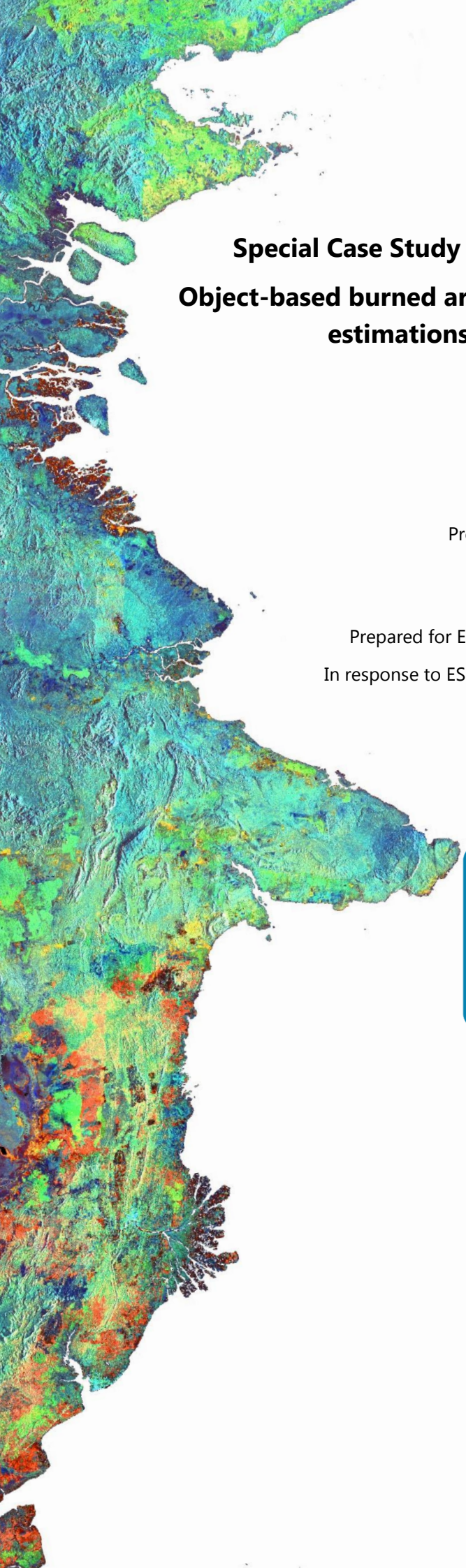

FIRE_CCI

Special Case Study on Fires in Indonesia and El Niño:

Object-based burned area detection and related fire emission estimations based on Sentinel-1 data

D2

Product Validation Report

Prepared for European Space Agency (ESA-ESRIN)

In response to ESRIN/Contract No. 4000115006/15/I_NB

January 2017

Revision History

Deliverable	**D2**		
Work Package	Phase I		
Due date	KO+8		
Authors	Sandra Lohberger, Matthias Stängel, Florian Siegert		
Distribution	CCI-FIRE-EOPS-MM-16-0140		
Reason for change			
Issue			
Revision	2		
Date		12 January 2017	
Release	3		
Version	01		

Table of Contents

List of Tables

List of Figures

1 Executive summary

Indonesia's invaluable tropical forests are home to many endangered species, comprise high biodiversity and store huge amounts of carbon. However, these forests are threatened by wild fires each year during the dry season. A very severe El Niño hit Indonesia in 2015 and resulted in an extreme drought. Consequences were vast disastrous forest and peat fires.

The aim of this project is to estimate damage caused by these fires in Indonesia 2015/2016 using Sentinel-1 imagery. Comprehensive burned area maps derived from Sentinel-1 imagery are created for Indonesia's three largest islands, namely Sumatra (480,000 km^2), Kalimantan (536,000 km^2) (part of the island Borneo) and West-Papua (460,000 km^2) for the dry season of 2015 and 2016. The resulting burned area maps are validated using multispectral Sentinel-2 and Landsat-8 data of acceptable could coverage as well as using field information collected in alliance with GIZ in Sumatra. Fire emission estimates are then derived for the study period using existing carbon stock and land cover maps with corresponding emission factors.

The Product Validation Report describes the validation approaches as well as results of burned area assessment, pre-fire land cover and carbon emissions estimations conducted within this study.

2 Introduction

Vast and disastrous forest and peat fires were raging across Indonesia in 2015 putting Indonesia on track to be one of the world's largest carbon emitters this year. Especially peat fires are smouldering underground and produce thick haze drifting to neighbouring countries Malaysia, Singapore and Thailand. The thick haze causes not only economic harm but also health issues caused by the pollution: The Pollutant Standards Index (PSI) is an air quality index which broadly exceeded values of 300 which represent "hazardous" air quality. In Central Kalimantan, an alarming PSI value of 1,801 was recorded on 1st October 2015. It is assumed that the fires are mostly started deliberately and illegally for large-scale plantation development for pulpwood and oil palm. The drainage of peatland areas increases the susceptibility to fires which is further enhanced by strong El Niño episodes causing a prolonged drought period. In 2015, the region was experiencing a very strong El Niño climate phenomenon. Recent estimates from the Global Emission Fire Database indicate that Indonesia's fire emissions from 2015 are estimated at 1.75 Gt of carbon [1].

These estimates contain a substantial amount of uncertainty related to the complex fire situation and the fact that they are based on fire detections derived from MODIS. NASA's two MODIS satellites Aqua and Terra make active fire data available every day by applying a fire and thermal anomalies algorithm [2]. Thermal anomalies or active fires represent the centre of a 1 km^2 pixel containing one or more fires within the pixel. This is the most basic fire product in which active fires and other thermal anomalies, such as volcanoes, are identified. However, thick haze and clouds prevent the detection of active fires which in turn result in substantial underestimation of fire events (see Figure 1). Fires were only detected in areas where the blanket of haze was thin enough.

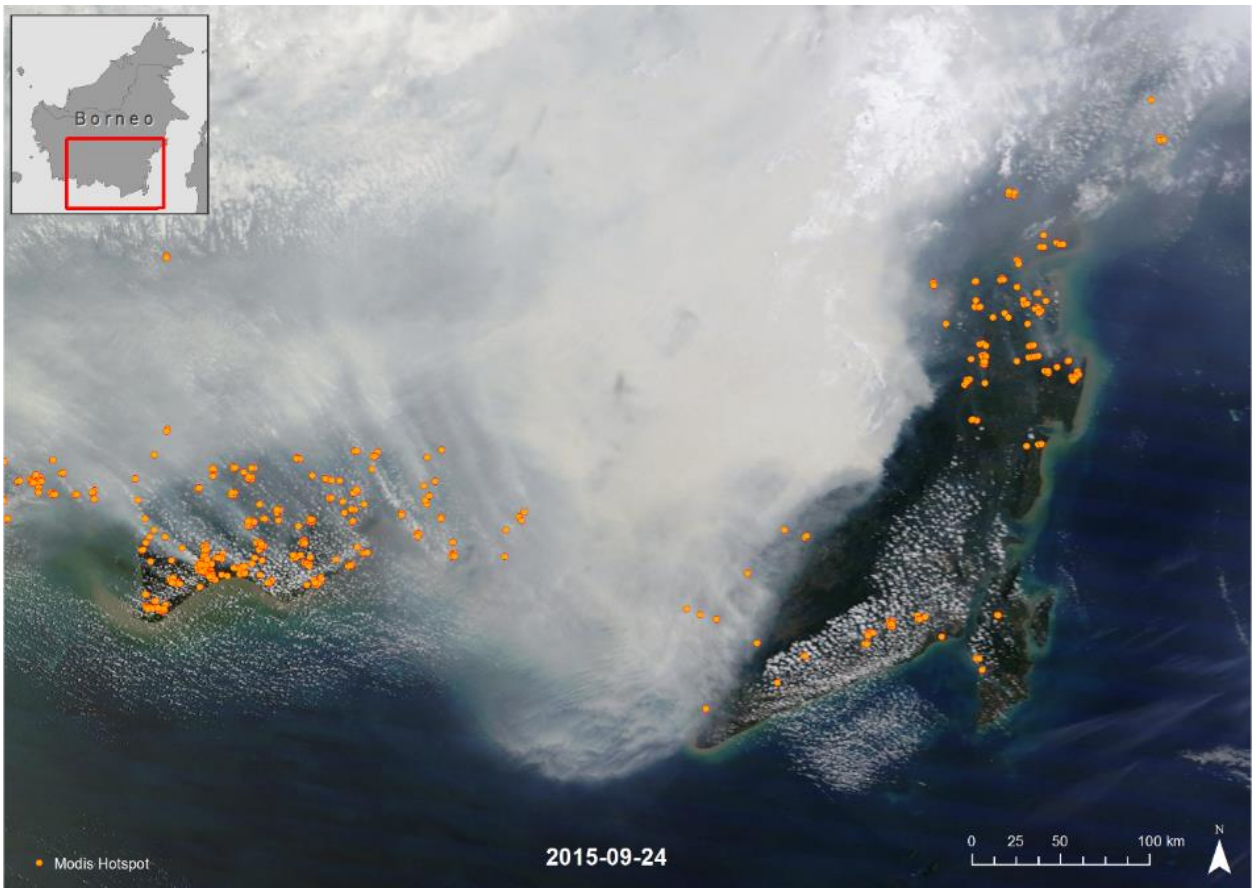

Figure 1: MODIS imagery and hotspot data from 24 September 2015 showing that thick haze from wildfires on Borneo.

In an attempt to monitor and contain these fires, ground teams assess the extent and intensity of fire damage. Nevertheless, their reports describe difficulties in measuring impacts onsite and underline the need for additional management techniques. In contrast, remote sensing approaches appear to present a viable solution for fire management. The European C-band SAR satellite Sentinel-1 can penetrate thick haze and detect damage caused by recent fires on the ground. Similarly, valuable multispectral imagery of regions before and after fires can be acquired by Sentinel-2, in order to complete time series analyses.

The aim of this project is to estimate the damage caused by the fire catastrophe 2015 in Indonesia and related fire emissions as well as for the year 2016. Comprehensive burned area maps derived from Sentinel-1 imagery are created for fire prone areas in the three largest islands of Indonesia (Sumatra, Kalimantan and West Papua). An object-based classification approach for Sentinel-1 was developed which detects the disturbance between two time steps, one before and one after the fire. The resulting burned area maps are then validated on the one hand by using Sentinel-2 and Landsat-8 data of acceptable cloud coverage, and on the other hand based on in-situ data collected in alliance with the GIZ (German Corporation for International Cooperation) for Sumatra. Previous work has shown that burn scars can be identified with high accuracy in Landsat or Sentinel-2 imagery using an object-based classification approach [3]. Emission estimates will be derived for the study period, using methodologies developed for and presented in Borneo's GlobBiomass study or existing land cover maps such as CCI Land Cover or Indonesian Ministry of Environment and Forestry (MoEF) land cover maps with corresponding emission factors. These existing land cover maps are cross-compared with a separately produced land cover map on a 100.000 km^2 study site.

3 Methods

3.1 Sentinel-1 burned area validation

Burned areas classified on the basis of Sentinel-1 imagery (see D1 Algorithm Theoretical Basis Document - ATBD [4]) were validated using in-situ GPS, ground and aerial photo information (collected in collaboration with GIZ in Sumatra), Sentinel-2 and Landsat-8 data. Sentinel-2 and Landsat-8 imagery were acquired on designated areas where cloud coverage allows comprehensive burned area detection (Figure 2). These areas were assigned to specific validation sites (S1, B1-6, P1-6). Scenes acquired shortly after the fire season (approximately until December) were used as burn scars are detected with higher confidence (Table 1). If the time delay is too large then fast regrowth of vegetation impedes the detection of burned areas (Figure 3). All images were pre-processed including geometric, radiometric and atmospheric correction as described in the ATBD [4]. Additionally, Sentinel-2 imagery will be automatically classified for burned areas by an object-based classification approach and compared to burned area classifications derived from Sentinel-1.

Figure 2: Locations of validation sites where Sentinel-2 and Landsat-8 data with relatively low cloud coverage was acquired shortly after the fire season.

Table 1: Overview of used Sentinel-2 and Landsat-8 imagery for validation and accuracy assessment. The locations of the validations site are depicted in Figure 2.

Region	Validation site	Sensor	Acquisition date	Scene name
Sumatra	S1	Landsat-8	01/11/2015	LC81240632015305LGN00
Borneo	B1	Sentinel-2	26/12/2015	S2A_20151226...T49MFT
	B2	Sentinel-2	26/12/2015	S2A_20151226...T49MET
	B3	Sentinel-2	26/12/2015	S2A_20151226...T49MFS
	B4	Sentinel-2	26/12/2015	S2A_20151226...T49MGS
	B5	Landsat-8	31/10/2015	LC81170582015304LGN00
	B6	Sentinel-2	23/12/2015	S2A_20151223...T50MLB
Papua	P1	Landsat-8	19/11/2015	LC81060622015323LGN00
	P2	Landsat-8	18/10/2015	LC81060602015291LGN00
	P3	Landsat-8	11/10/2015	LC81050612015284LGN00
	P4	Sentinel-2	03/12/2015	S2A_20151203...T53LQG
	P5	Sentinel-2	03/12/2015	S2A_20151203...T53LRG
	P6	Sentinel-2	30/11/2015	S2A_20151130...T54LVM

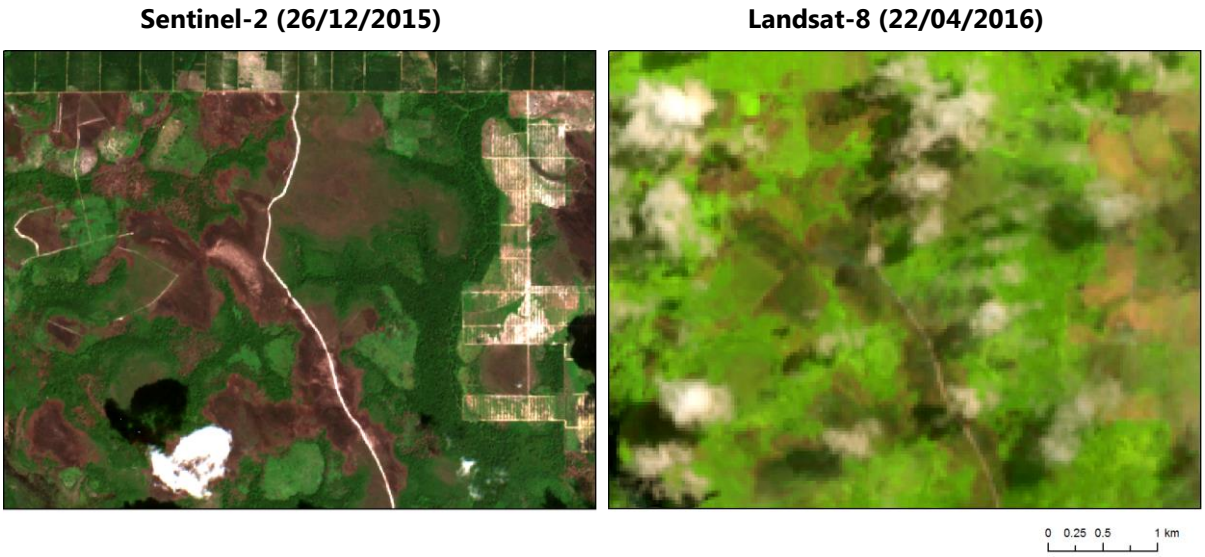

Figure 3: Example of fast regrowth which hampers the detection of burn scars approximately four months later.

3.1.1 Accuracy assessment of Sentinel-1 burned areas

In-situ information, collected in April 2016 within the GIZ BIOCLIME project area in Sumatra, together with Sentinel-2 and Landsat-8 imagery served as reference data for accuracy assessment of burned area classifications derived from Sentinel-1.

An independent accuracy assessment and verification of the classification results with reference data is an essential component of the processing chain. The accuracy analysis provides an accuracy matrix considering user's and producer's accuracies, the overall accuracy and the Kappa index.

An accuracy matrix compares the land cover information from the reference samples to the classification results. The overall accuracy shows the percentage of correctly classified reference samples among all reference samples, the producer's accuracy indicates how well the reference site given cover type is classified and the user's accuracy on the other hand indicates the probability that a pixel classified into a given category actually represents that category on the ground. Finally, the Kappa index serves as an indicator of the extent to which the percentage correct values of an accuracy matrix are due to "true" agreement versus "chance" agreement [5].

When choosing the amount of samples to be collected for the subsequent accuracy assessment a balance what is statistically sound and what is practically attainable must be found. General guidelines for accuracy assessment of remotely sensed data suggest that the minimum number of samples should be at least 50 per category/land cover class [6].

In addition, the choice and distribution of the samples (sampling scheme) is an important component of an accuracy assessment. Five different sampling schemes are common [6]:

- **Simple random sampling:** Here each sample unit in the study area has an equal chance of being selected. Main advantage here is the good statistical properties that result from the random selection of samples.
- **Systematic sampling:** Here the sample units are selected at some equal interval over the study area. Main advantage here is the ease in sampling somewhat uniformly over the whole study area.
- **Stratified random sampling:** The sampling scheme is similar to simple random sampling only that prior knowledge of the study area is used to divide the area into groups or strata (classes) and then each stratum (class) is randomly sampled. The main advantage here is that all strata (classes), no matter how small, will be included.
- **Cluster sampling:** This sampling scheme is frequently used in assessing the accuracy of remotely sensed data, especially to collect information on many samples quickly.
- **Stratified systematic unaligned sampling:** Here it is attempted to combine the advantages of randomness and stratification with the ease of a systematic sampling without the common problems arising when applying systematic sampling.

Therefore, we decided to use all available in-situ information and apply stratified random sampling for each validation site with multispectral imagery using a sample size of 50. In-situ data include GPS locations, geo-referenced ground photos and aerial drone data which were categorized into the classes "burned" and "not burned". Figure 4 shows the locations and examples of collected in-situ information in South Sumatra in April 2016. The photos depict examples that were used and categorized into the classes "burned" and "not burned". Multispectral imagery (Sentinel-2 and Landsat-8) was visually categorized into the classes "burned" and "not burned" for each of the 1,300 stratified random sampling points. The validation was solely based on visual interpretation of satellite images at the sampling points as the automatic classification (see 3.1.2) was not accurate enough for validation purposes. The locations of the validation sites are shown in Figure 2.

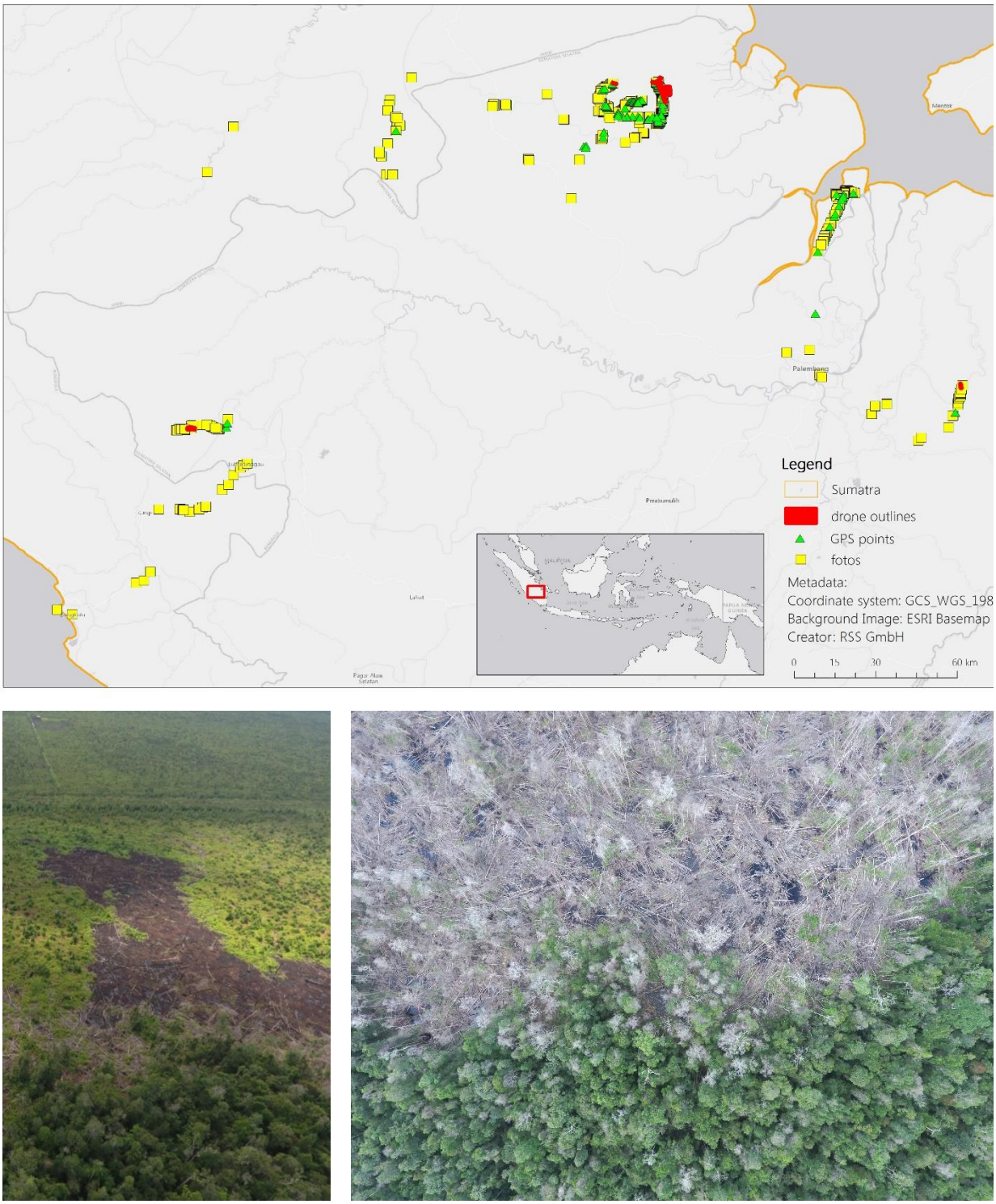

Figure 4: Locations of in-situ data collected in collaboration with GIZ in South Sumatra. The photos show examples of burned and adjacent not burned areas.

3.1.2 Automatic burned area classification comparison of SAR and multispectral data

Sentinel-2 and Landsat-8 images were pre-processed as described in the ATBD [4] and processed by an object-based classification method with a hierarchical rule-set. This approach classifies spatially adjacent pixels as a group of pixels with similar spectral characteristics (image objects). Burned areas were classified per validation site in relatively cloud free regions (see Figure 2) on the basis of different burn

ratio indices. Previous work has shown that these ratios are capable to detect burned areas in Landsat scenes over cloud and haze free areas (see Figure 5) and this approach was adapted to Sentinel-2 imagery [7]. Areas covered by clouds, cloud shadow or topographic shadow will not allow a detection of burned areas with this method and were therefore excluded.

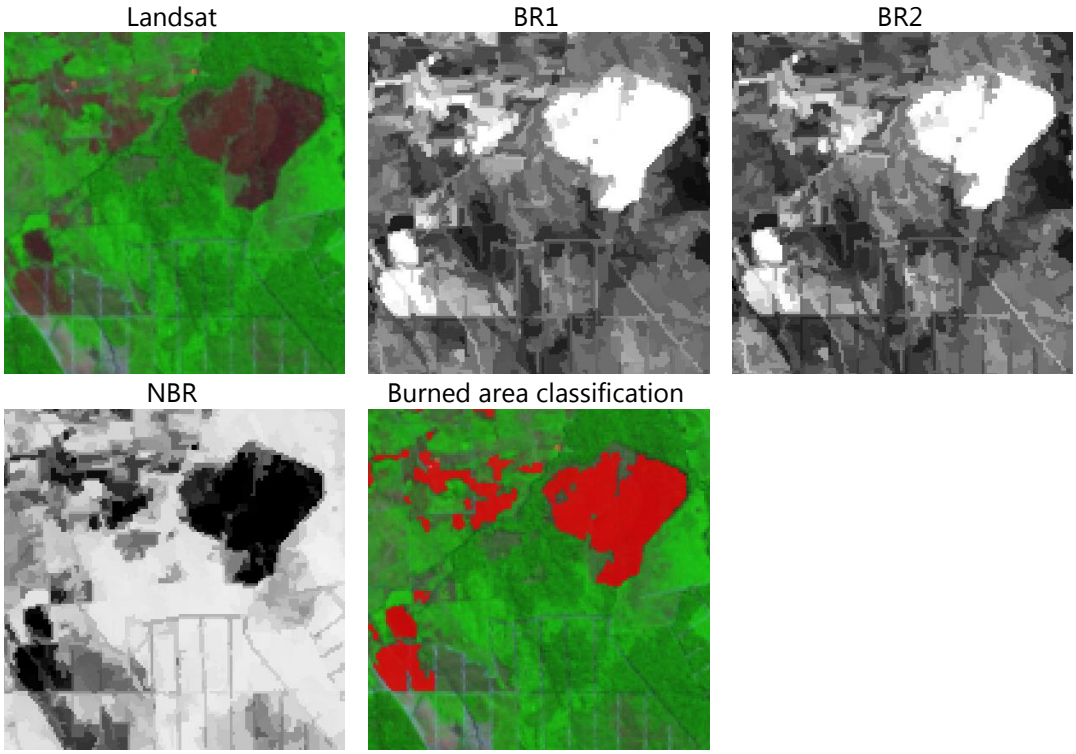

Figure 5: Landsat image with corresponding burn ratio 1 (BR1), burn ratio 2 (BR2), and normalized burn ratio (NBR) used for automatic burned area classification.

Burned areas were classified per validation site with ratios based on bands $b_{0.84\mu m}$, $b_{2.22\mu m}$, and $b_{11.45\mu m}$:

- $BR1 = (b_{0.84\mu m} - b_{11.45\mu m}) / (b_{0.84\mu m} + b_{11.45\mu m})$ (eq. 1)

where $b_{0.84\mu m}$ is the reflectance value of Near Infrared (0.76-0.90 µm) and $b_{11.45\mu m}$ is the reflectance value of Thermal Infrared (10.4-12.5µm).

- $BR2 = (b_{0.84\mu m} - b_{2.22\mu m}) / (b_{0.84\mu m} + b_{11.45\mu m})$ (eq. 2)

where $b_{0.84\mu m}$ is the reflectance value of Near Infrared (0.76-0.90 µm), $b_{2.22\mu m}$ is the reflectance value of Mid-Infrared (2.08-2.35 µm) and $b_{11.45\mu m}$ is the reflectance value of Thermal Infrared (10.4-12.5µm).

- $NBR = (b_{0.84\mu m} - b_{2.22\mu m})/(b_{0.84\mu m} + b_{2.22\mu m})$ (eq. 3)

where $b_{0.84\mu m}$ is the reflectance value of Near Infrared (0.76-0.90 µm) and $b_{2.22\mu m}$ is the reflectance value of Mid-Infrared (2.08-2.35 µm).

The burned area classification from multispectral imagery was conducted on all images listed in Table 1 by finding appropriate threshold values for BR1, BR2 and NBR for each scene and quantitatively compared to Sentinel-1 burned area classifications.

A classification of burned area using the ABAMS software by the University of the Basque Country, as suggested in D2.1 – Product Validation Plan [8], was not implemented in the validation workflow due to the frequent cloud coverage over the study region. The ABAMS software requires cloud-free pre- and post-fire imagery which was not applicable in the study region.

3.2 Emission and damage assessment

In order to evaluate both fire emission estimations derived from CCI and MoEF land cover (see ATBD [4]), an independent pre-fire land cover classification was conducted on the basis of Landsat-8 for a designated area in South Sumatra of app. 100.000 km^2. A special focus was paid to distinguish different forest types with regard to different carbon storage. The classification approach is described in the ATBD [4].

It is assumed that the produced land cover classification is more accurate than existing, available land cover maps (CCI and MoEF) in terms of resolution and land cover class distinction. Therefore, the calculated emissions were compared on basis of estimated emission of the produced land cover classification. The approach to calculate vegetation and peat fire emissions is described in the ATBD [4].

4 Results

4.1 Sentinel-1 burned areas

4.1.1 Mapped burned areas

Figure 6 shows mapped burned areas derived from Sentinel-1 in Sumatra, Kalimantan and Papua (Indonesia) for 2015. Most fires are located in the southern part of Kalimantan, the south-eastern part of Sumatra and the southern part of Papua. The total burned area for the three regions in 2015 is estimated at 4,604,569 ha. Approximately half of mapped burned areas are located in Kalimantan with 2,268,352 ha whereas in Sumatra 1,518,127 ha were classified as burned and in Papua 818,090 ha.

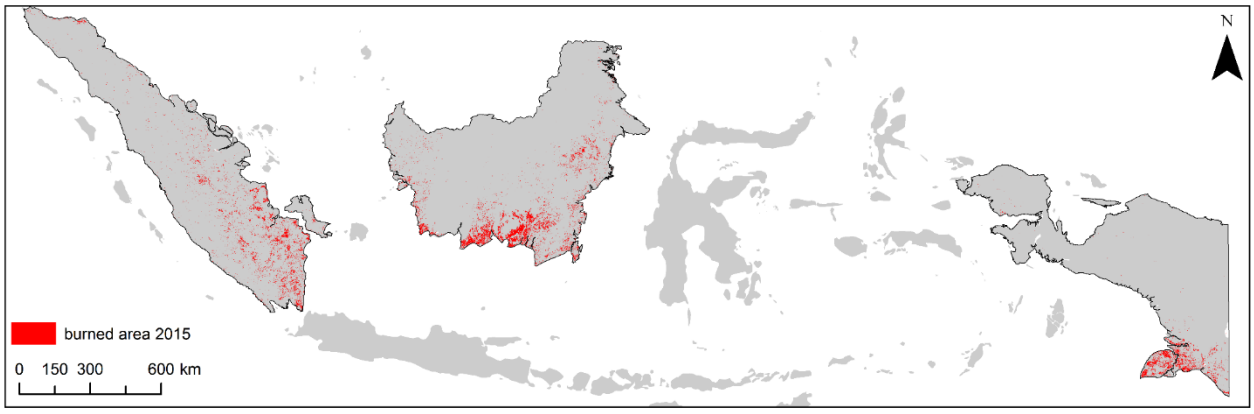

Figure 6: Spatial distribution of Sentinel-1 burned areas in 2015.

In total, 37% of classified burned areas was on peat of which approximately half were in Kalimantan. Table 2 shows the total burned area derived from Sentinel-1 for the three regions categorized by areas on peat and not on peat. Considering fires on peat is very crucial for fire emission estimation (see ATBD [4]).

Table 2: Total burned areas derived from Sentinel-1 imagery on peat and not on peat based on Wetlands International peat layer.

	Sumatra	Kalimantan	Papua	Total
burned not on peat [ha]	1,161,692.80	1,455,200.12	283,473.50	2,900,366.41
burned on peat [ha]	356,434.47	813,151.75	534,616.01	1,704,202.23
Total burned area [ha]	1,518,127.26	2,268,351.87	818,089.51	**4,604,568.65**

4.1.2 Accuracy assessment

In total, 138 GPS locations, 1,631 photos and 145 drone samples were available and used for Sentinel-1 burned area accuracy assessment. The GPS locations and the geolocated photos were carefully selected regarding their position in the field. Only points within burned areas larger than the MMU were selected. Additionally, the spatial inaccuracy of the respective GPS device was taken into account in the selection of the validation points. The GPS locations resulted in an overall accuracy of 77.54%, the photo validation in 84.92% and drone data in 80.69%. The following tables show the error matrices for in-situ validation of delineated burned areas including user's and producer's accuracy as well as the kappa index (Table 3, Table 4, Table 5).

Table 3: Error matrix for Sentinel-1 burned area classification based on GPS locations shown in Figure 4.

		GPS			
		burned	not burned	**total**	***User's accuracy***
mapped burned area	burned	**59**	9	**68**	*86.76*
	not burned	22	***48***	**70**	*68.57*
	total	**81**	**57**	*Correct=107* *Total samples=138* ***Overall acc.=77.54%*** ***Kappa=0.77***	
	Producer's Accuracy	*72.84*	*84.21*		

Table 4: Error matrix for Sentinel-1 burned area classification based on ground photos (Figure 4).

		Photos			
		burned	not burned	**total**	***User's accuracy***
mapped burned area	burned	**277**	132	**409**	*67.73*
	not burned	114	***1108***	**1222**	*90.67*
	total	**391**	**1240**	*Correct=1,385* *Total samples=1,631* ***Overall acc.=84.92%*** ***Kappa=0.85***	
	Producer's Accuracy	*70.84*	*89.35*		

Table 5: Error matrix for Sentinel-1 burned area classification based on drone data (Figure 4).

		Drone			
		burned	not burned	**total**	***User's accuracy***
mapped burned area	burned	**70**	3	**73**	*95.89*
	not burned	25	***47***	**72**	*65.28*
	total	**95**	**50**	*Correct=117* *Total samples=145* ***Overall acc.=80.69%*** ***Kappa=0.81***	
	Producer's Accuracy	*73.68*	*94.00*		

Within each validation site, 50 samples were randomly distributed within and outside mapped burned areas, respectively. Table 6 shows the overall confusion matrix including user's and producer's accuracy for each validation site. The locations of the validation sites are shown in Figure 2. The validation of classified burned areas using multispectral imagery resulted in an overall accuracy of 83.54%.

Table 6: Error matrix for visual multispectral accuracy assessment of Sentinel-1 burned areas. Validation sites are depicted in Figure 2.

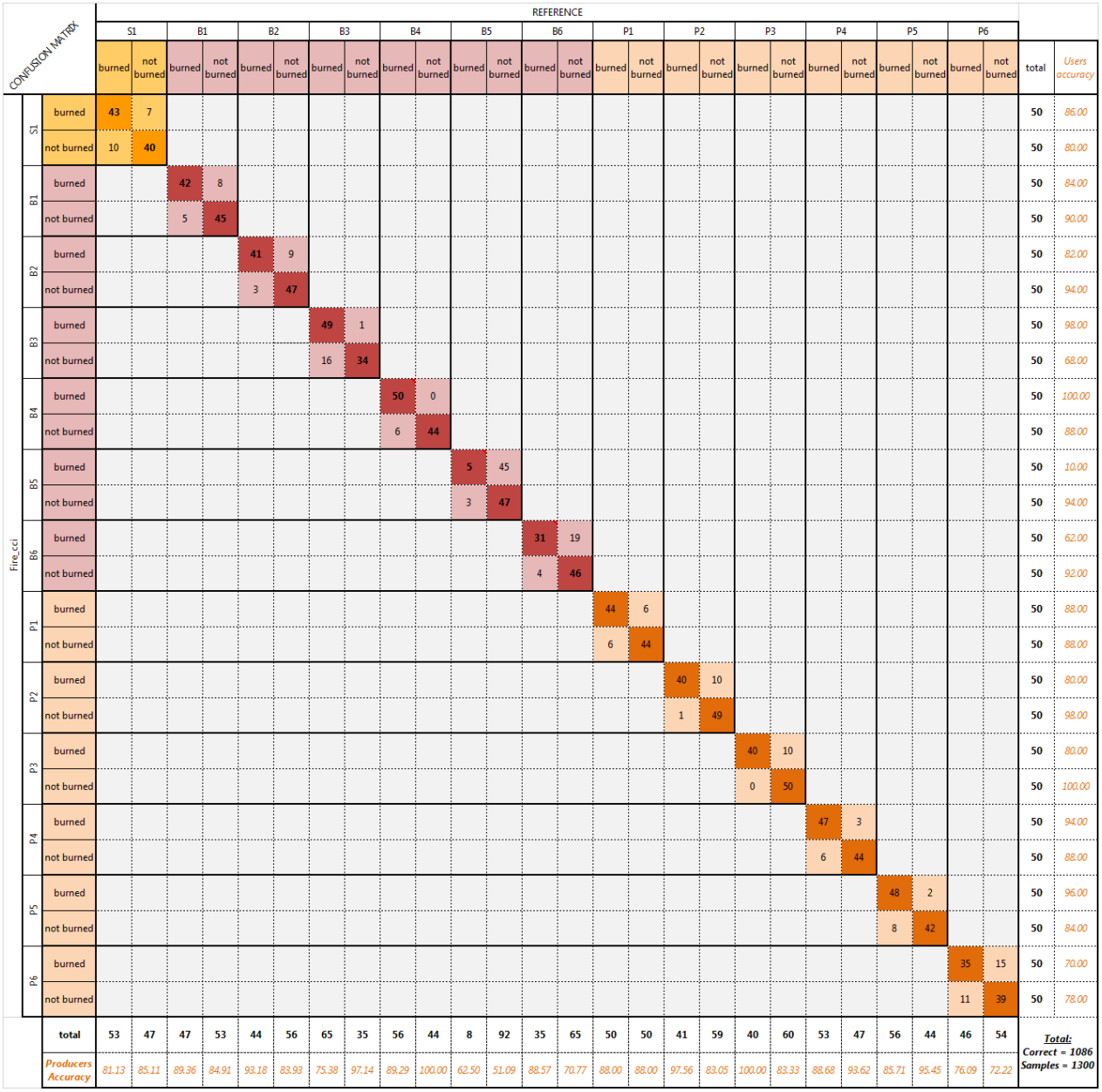

CONFUSION MATRIX		REFERENCE																											
		S1		B1		B2		B3		B4		B5		B6		P1		P2		P3		P4		P5		P6			
		burned	not burned	burned	not burned	burned	not burned	burned	not burned	burned	not burned	burned	not burned	burned	not burned	burned	not burned	burned	not burned	burned	not burned	burned	not burned	burned	not burned	burned	not burned	total	Users accuracy
Fire_cci	S1 burned	43	7																									50	86.00
	S1 not burned	10	40																									50	80.00
	B1 burned			42	8																							50	84.00
	B1 not burned			5	45																							50	90.00
	B2 burned					41	9																					50	82.00
	B2 not burned					3	47																					50	94.00
	B3 burned							49	1																			50	98.00
	B3 not burned							16	34																			50	68.00
	B4 burned									50	0																	50	100.00
	B4 not burned									6	44																	50	88.00
	B5 burned											5	45															50	10.00
	B5 not burned											3	47															50	94.00
	B6 burned													31	19													50	62.00
	B6 not burned													4	46													50	92.00
	P1 burned															44	6											50	88.00
	P1 not burned															6	44											50	88.00
	P2 burned																	40	10									50	80.00
	P2 not burned																	1	49									50	98.00
	P3 burned																			40	10							50	80.00
	P3 not burned																			0	50							50	100.00
	P4 burned																					47	3					50	94.00
	P4 not burned																					6	44					50	88.00
	P5 burned																							48	2			50	96.00
	P5 not burned																							8	42			50	84.00
	P6 burned																									35	15	50	70.00
	P6 not burned																									11	39	50	78.00
	total	53	47	47	53	44	56	65	35	56	44	8	92	35	65	50	50	41	59	40	60	53	47	56	44	46	54	Total: Correct = 1086 Samples = 1300	
	Producers Accuracy	81.13	85.11	89.36	84.91	93.18	83.93	75.38	97.14	89.29	100.00	62.50	51.09	88.57	70.77	88.00	88.00	97.56	83.05	100.00	83.33	88.68	93.62	85.71	95.45	76.09	72.22		

Overall Accuracy	83.54%
Kappa	0.84

Combining in-situ and multispectral validation samples, an overall accuracy of 83.85% and kappa index of 0.84 was achieved (Table 7).

Table 7: Error matrix for all available validation samples consisting of in-situ and multispectral reference data.

		all validation data			
		burned	not burned	**total**	***User's accuracy***
mapped burned area	burned	**921**	279	**1200**	*76.75*
	not burned	240	***1774***	**2014**	*88.08*
	total	**1161**	**2053**	*Correct=2695* *Total samples=3214* ***Overall acc.=83.85%*** ***Kappa=0.84***	
	Producer's Accuracy	*79.33*	*86.41*		

4.1.3 Automatic burned area classification comparison of SAR and multispectral data

Each validation site was automatically classified for burned areas based on multispectral imagery and compared to the results obtained from SAR Sentinel-1 data. Table 8 depicts an overview of automatically mapped burned areas based on multispectral data (Sentinel-2 and Landsat-8) or SAR Sentinel-1 imagery. The multispectral acquisition date, the total area of the validation site, the cloud coverage in multispectral imagery as well as detected burned areas using multispectral and SAR data, respectively, is shown. These numbers are illustrated in the graph in Figure 7 in order to compare both numbers of detected burned areas. The graph also emphasises the difficulty to compare both dataset for automatic burned area assessment due to acquisition time difference and cloud coverage.

Table 8: Comparison of mapped burned areas on the basis of multispectral or Sentinel-1 imagery.

Region	**Validation site**	**Sensor**	**multispectral acquisition date**	**SAR pre-fire acquisition date**	**SAR post-fire acquisition date**	**Total area**	**Multispectral burned area**		**Cloud coverage**		**Sentinel-1 burned area**	
						[ha]	**[ha]**	**[%]**	**[ha]**	**[%]**	**[ha]**	**[%]**
Sumatra	S1	L-8	01/11/2015	26/06/2015	24/10/2015	1,959,549	16,239	0.8%	119,454	6.1%	98,187	5.0%
Borneo	B1	S-2	26/12/2015	01/07/2015	05/10/2015	88,455	4,427	5.0%	13,683	15.5%	826	0.9%
	B2	S-2	26/12/2015	01/07/2015	05/10/2015	97,747	831	0.9%	15,107	15.5%	95	0.1%
	B3	S-2	26/12/2015	01/07/2015	05/10/2015	217,399	32,089	14.8%	58,296	26.8%	60,510	2.8%
	B4	S-2	26/12/2015	20/07/2015	24/10/2015	56,446	5,688	10.1%	22,842	40.5%	15,793	28.0%
	B5	L-8	31/10/2015	27/07/2015	31/10/2015	339,101	4,601	1.4%	132,024	38.9%	2,292	0.7%
	B6	S-2	23/12/2015	27/07/2015	31/10/2015	198,768	8,703	4.4%	13,652	6.9%	19,114	9.6%
Papua	P1	L-8	19/11/2015	28/06/2015	19/11/2015	851,795	2,326	0.3%	616,920	7.2%	586	0.1%
	P2	L-8	18/10/2015	28/06/2015	19/11/2015	343,044	1,987	0.6%	84,922	24.8%	453	0.1%
	P3	L-8	11/10/2015	05/07/2015	09/10/2015	112,719	145	0.1%	10,628	9.4%	12	0.0%
	P4	S-2	03/12/2015	30/06/2015	28/10/2015	50,263	1,420	0.3%	11,227	22.3%	22,191	44.1%
	P5	S-2	03/12/2015	30/06/2015	28/10/2015	312,759	5,369	1.7%	145,593	46.6%	81,622	26.1%
	P6	S-2	30/11/2015	07/07/2015	04/11/2015	757,354	37,196	4.9%	240,210	3.2%	64,953	8.6%

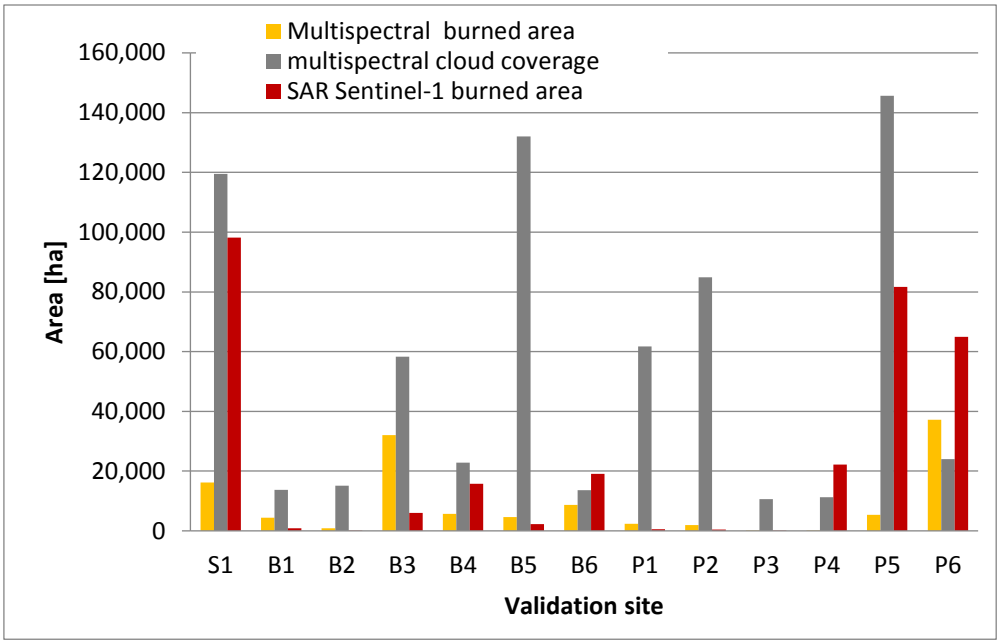

Figure 7: Burned area and cloud coverage for multispectral and SAR automatic burned area assessment.

Figure 8 shows burned areas for each validation site from the automatic classification approach using Sentinel-2/Landsat-8 or Sentinel-1 data.

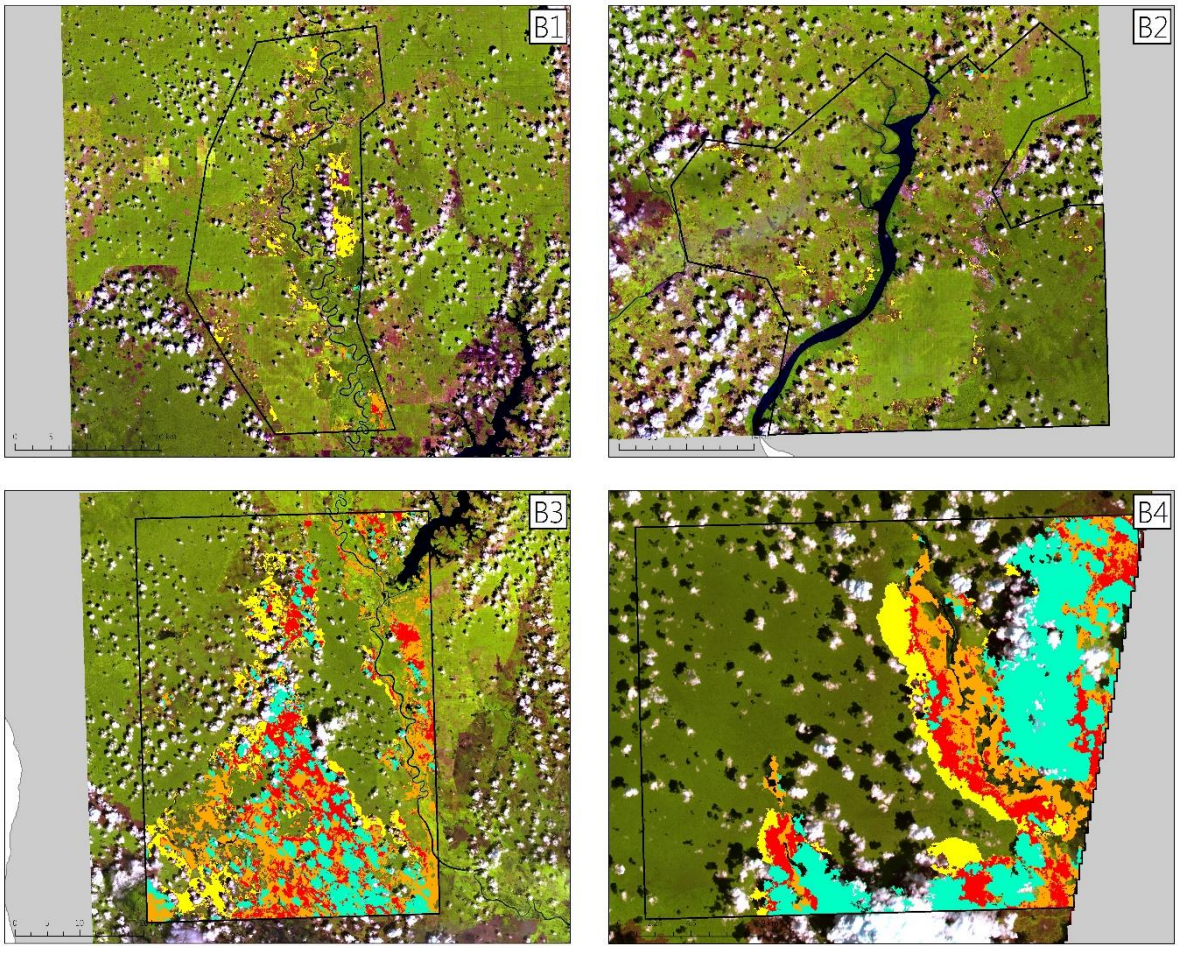

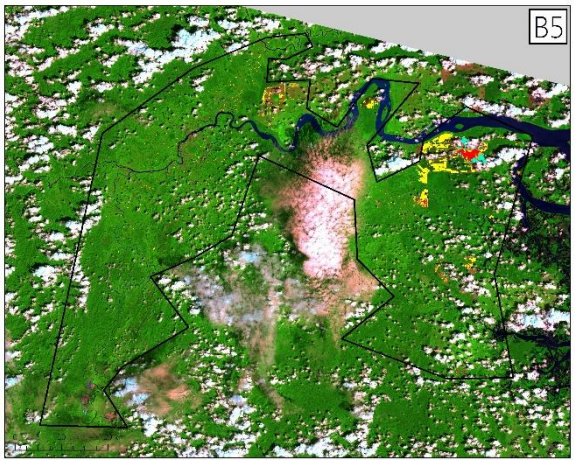
B5

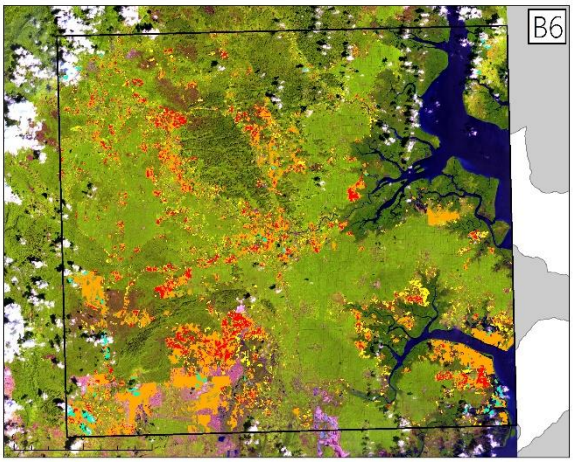
B6

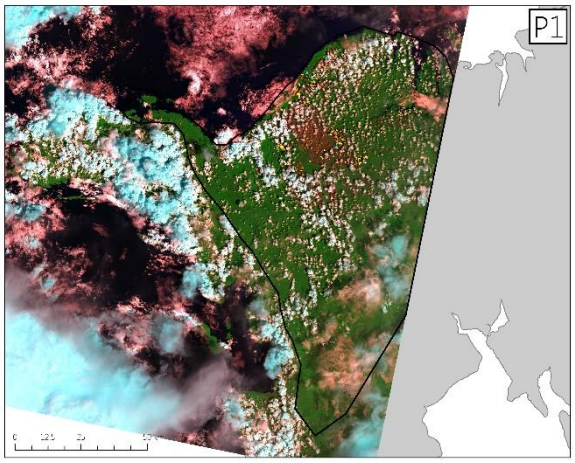
P1

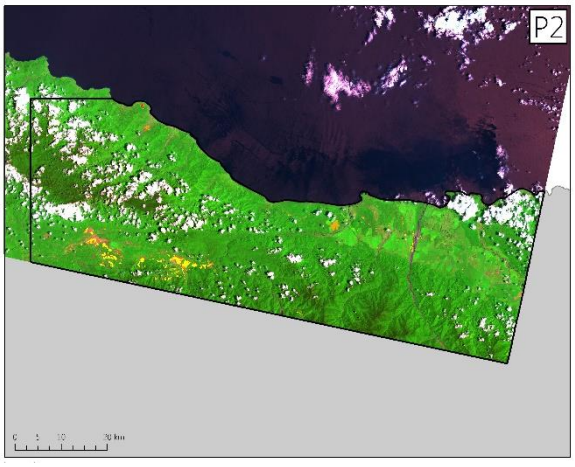
P2

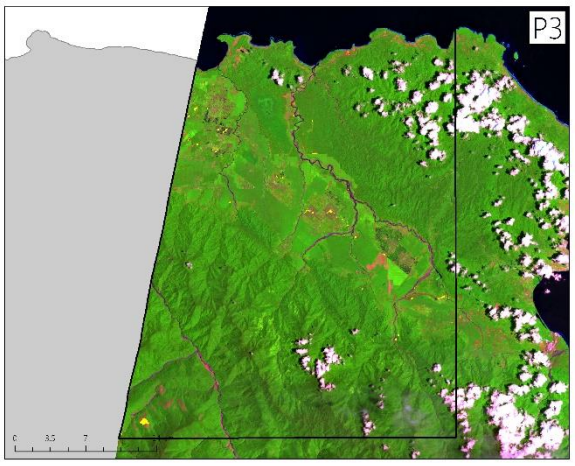
P3

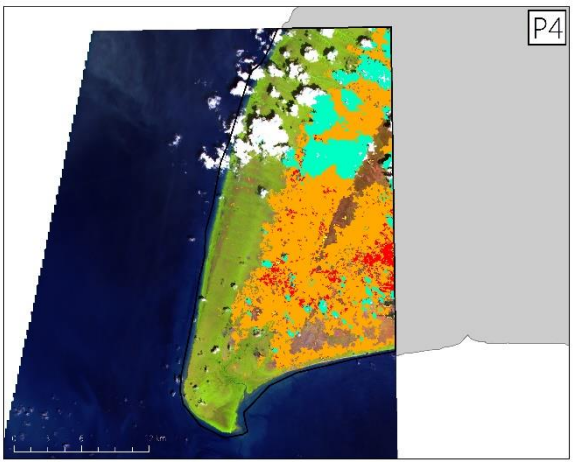
P4

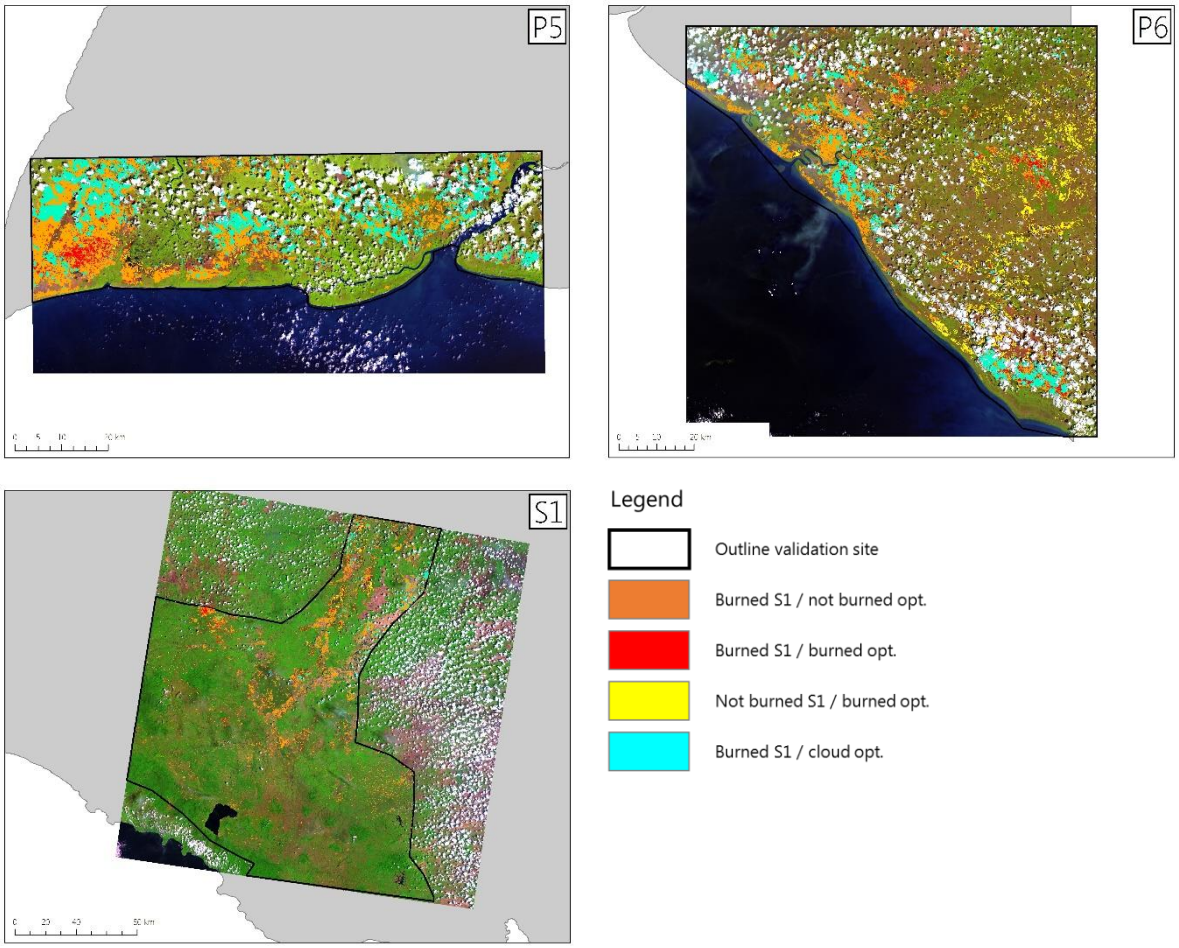

Figure 8: Comparison of automatically classified burned area derived from Sentinel-1 or Sentinel-2/Landsat-8 imagery for each validation site.

4.2 Emission estimation

Table 8 provides an overview of different emission estimation for Sentinel-1 burned areas based on different datasets described in the ATBD [4]. Vegetation fire emissions were estimated at 501.8 Mt CO_2-eq using MoEF and 1,117.3 Mt CO_2-eq using ESA CCI land cover classification for the whole study area. Belowground emissions were based on Wetland International peat layer and discriminated in first and more than one fire and resulted in 389 Mt CO_2-eq and 858 Mt CO_2-eq, respectively. This sums up to total fire emissions of 890 CO_2-eq and 1,975 CO_2-eq, respectively, in 2015 for the three regions. Figure 9 provides a graphical presentation of the results.

Furthermore, a reference land cover classification for an area of 100,000 km² for 2015 pre-fire conditions was generated as described in the ATBD [4] which is based on Landsat and Spot data. The final map is depicted in Figure 10. This area serves as "reference" map for the emission estimations to the other land cover classifications (MoEF and CCI) (see Table 9).

Vegetation fire emissions in the 100,000 km² reference site were estimated at 52.36 Mt CO_2-eq using MoEF, 78.33 Mt CO_2-eq using ESA CCI and 72.82 Mt CO_2-eq using the reference land cover classification. Belowground emissions resulted in 38.36 Mt CO_2-eq, 64.70 Mt CO_2-eq and 46.26 Mt CO_2-eq, respectively. This sums up to total fire emissions of 90.72 CO_2-eq based on MoEF, 143.03 CO_2-eq based on CCI and 119.08 CO_2-eq based on the reference land cover classification (see Table 10).

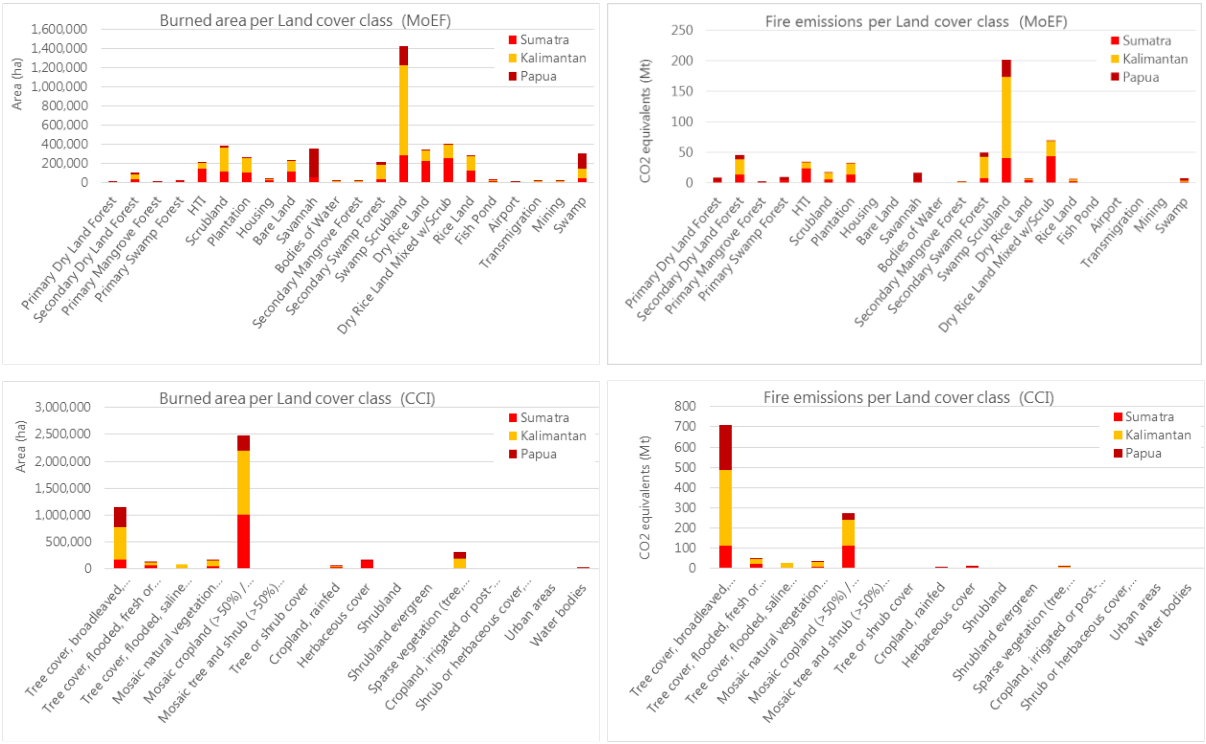

Figure 9: Mapped burned area for each land cover class on the basis of MoEF (upper panel) and CCI (lower panel) land cover classifications and related vegetation fire emissions for each region.

Table 9: Vegetation, peat and total fire emissions using different meta-datasets for Sentinel-1 derived burned areas.

		Emissions per region (Mt CO_2-eq)				
	Dataset	Sumatra	Kalimantan	Papua	**Total area**	100,000 km² reference site
Vegetation emissions	*GlobBiomass*	*n/a*	264.8	n/a	***n/a***	*n/a*
	MoEF	158.8	265.9	77.0	**501.8**	52.4
	CCI	271.4	583.3	262.5	**1,117.3**	78.33
	Reference	*n/a*	*n/a*	*n/a*	***n/a***	72.82
Peat emissions	*GlobBiomass*	*n/a*	198.4	*n/a*	***n/a***	*n/a*
	MoEF	95.8	184.6	108.2	**388.6**	38.36
	CCI	166.5	417.5	273.7	**857.8**	64.70
	Reference	*n/a*	*n/a*	*n/a*	***n/a***	46.26
Total emissions	*GlobBiomass*	*n/a*	463.1	*n/a*	***n/a***	*n/a*
	MoEF	254.7	450.5	185.2	**890.4**	90.72
	CCI	437.9	1,000.9	536.2	**1,975.0**	143.03
	Reference	*n/a*	*n/a*	*n/a*	***n/a***	119.08

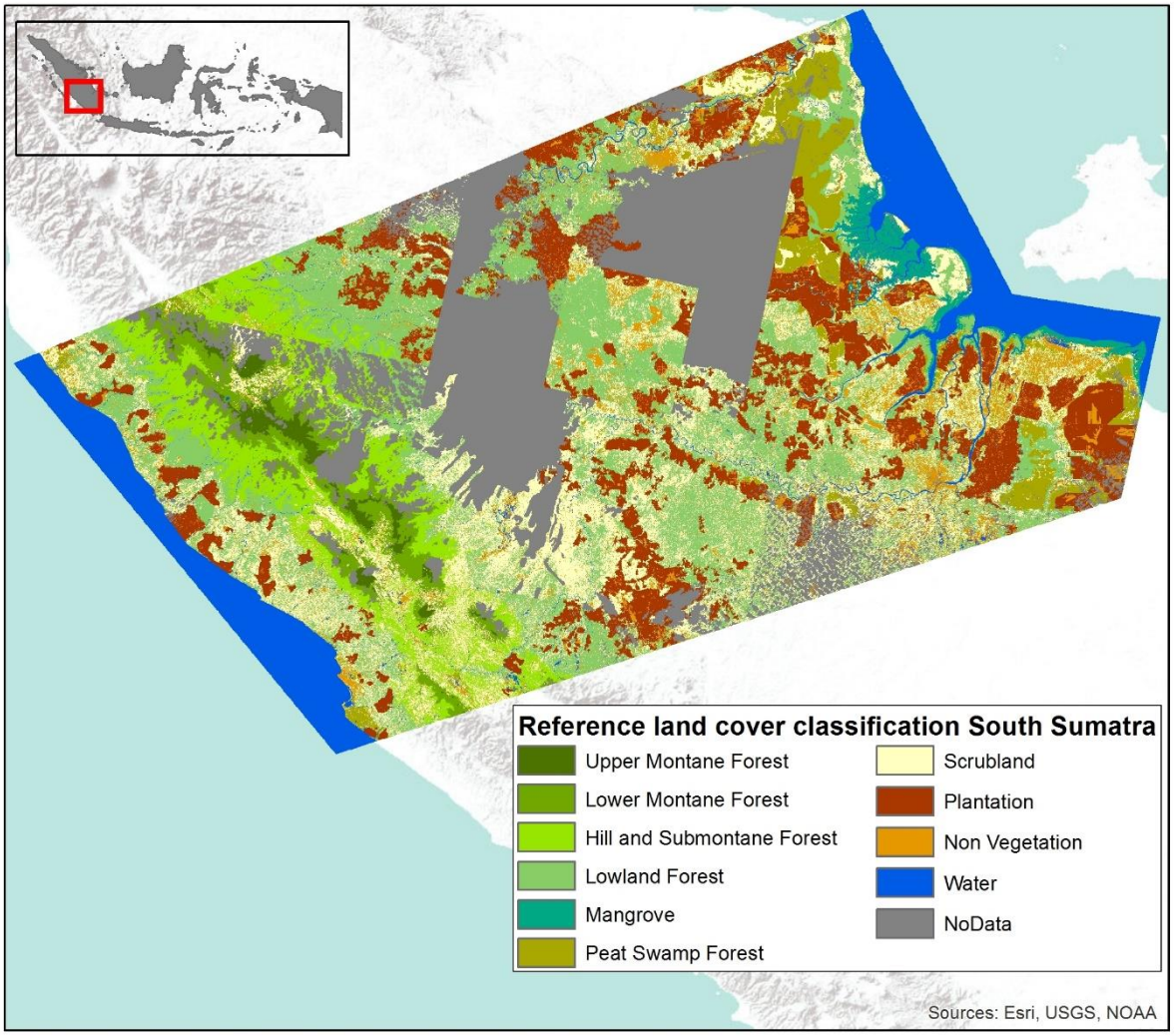

Figure 10: Final pre-fire reference land cover classification of the 100,000 km² reference site in South Sumatra. Grey NoData areas make up 20 % of the area which are due to cloud coverage during the rainy season when the data was collected.

Table 10: Comparison of fire emission estimations based on MoEF, CCI and the Reference land cover classification for the 100,000 km² reference site. Different emissions by vegetation and therefore by peat can be explained by the different land cover categories and definitions (see 5.2).

	Land cover classification		
	MoEF	CCI	Reference
Vegetation emissions [Mt CO_2-eq]	52.36	78.33	72.82
Peat emissions [Mt CO_2-eq]	38.36	64.70	46.26
Total emissions [Mt CO_2-eq]	90.72	143.03	119.08

4.3 PALSAR-2 cross comparison

For the cross comparison of PALSAR-2 and Sentinel-1 for automatic burned area mapping, an area with available data and similar acquisition dates in Central Kalimantan was selected covering 1,958,588 ha (Figure 9). The same pre-processing and classification approach was applied for PALSAR-2 (see ATBD [4]). The characteristics and main differences of both datasets are depicted in Figure 11.

The signal of the two datasets is completely different with regard to burned area detection. The backscatter signal of Sentinel-1 VV and VH polarization decreases after a fire event. The opposite happens for the PALSAR-2 backscatter signal where the backscatter signal increases in HH and HV polarization after a fire occurred.

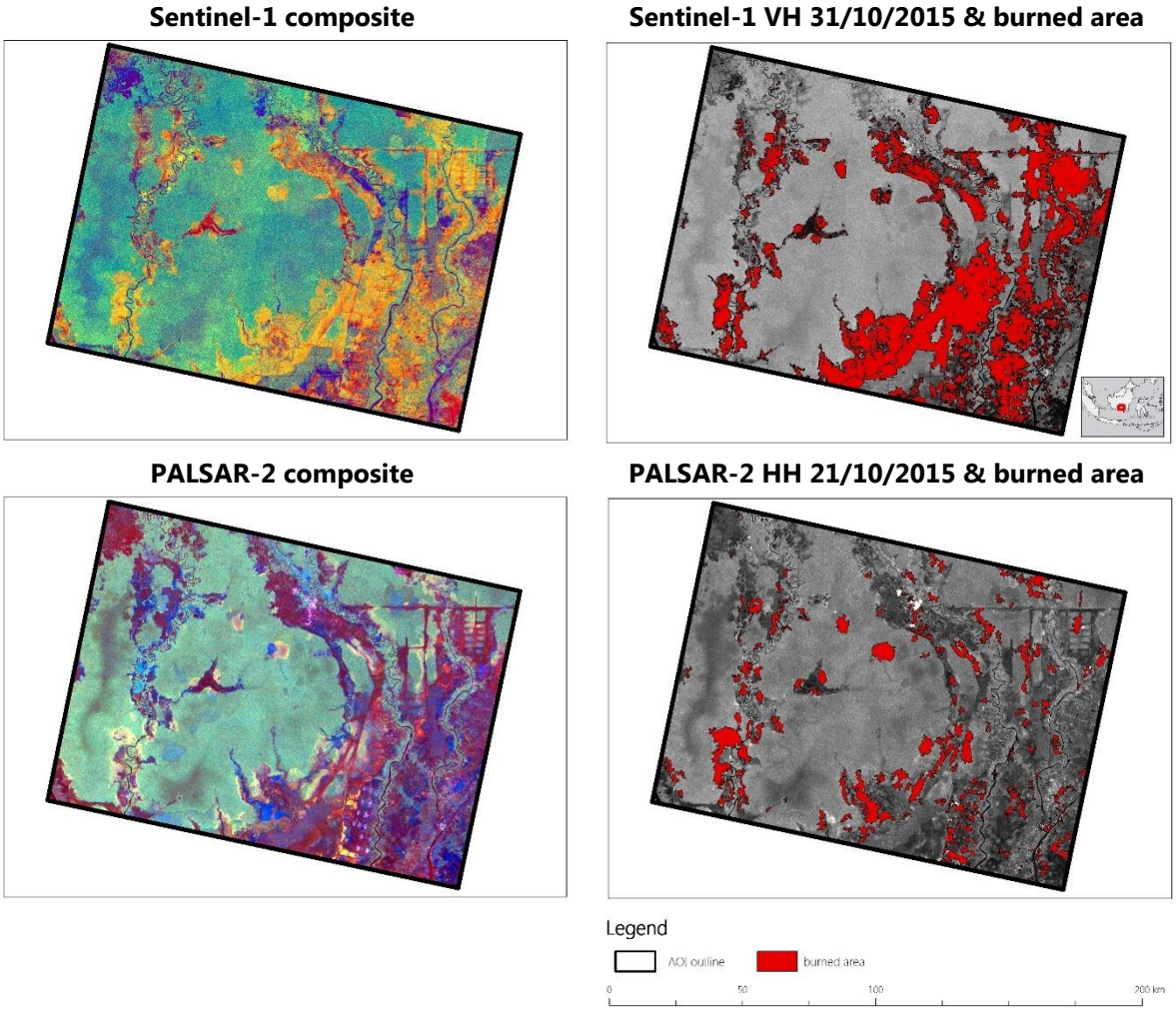

Figure 11: Sentinel-1 and PALSAR-2 false colour composite and classified burned areas.

The resulting burned area classification using Sentinel-1 is almost three times higher than using PALSAR-2. However, the pre-fire acquisition dates differ by three days (Sentinel-1 27/07/2015 vs. PALSAR-2 24/07/2015) and the post-fire acquisition dates differ by 10 days (Sentinel-1 31/10/2015 vs. PALSAR-2 21/10/2015). This difference is one reason for the different amount of mapped burned area. Having a look at the number of MODIS hotspots provides an indication of the number of fires that burned between the acquisition dates. In total 11,208 hotspots were detected within this area between 27/07/2015 and 31/10/2015. During the pre-fire acquisition date difference, 7 hotspots were recorded by MODIS and during the post-fire acquisition date difference, 975 hotspots were detected which could be only classified by Sentinel-1.

The visual comparison of the results to optical data shows that Sentinel-1 classifies burned areas with higher accuracy than PALSAR-2. An additional reason for this result is the different wavelength. The reduction of backscatter signal from forest to burned area is more concise in the C-band signal than in the L-band signal.

Table 11: Characteristics and classified burned areas using Sentinel-1 and PALSAR-2, respectively, for automatic burned area cross comparison.

	polarization	Spatial resolution	SAR	Pre-fire acquisition date	Post-fire acquisition date	classified burned area [ha]
Sentinel-1	VV & VH	10 m	C-band	27/07/2015	31/10/2015	466,147
PALSAR-2	HH & HV	25 m	L-band	24/07/2015	21/10/2015	151,081

5 Discussion

5.1 Automatic burned area classification

Burned areas derived from either multispectral or SAR imagery sometimes differed extremely in their extent which might be due to several reasons.

- **Time difference**: Multispectral scenes were acquired up to four months later than Sentinel-1 images as there was no other option in terms of cloud coverage and data availability. Some of the areas were still burning after the Sentinel-1 acquisition and some areas have already experienced some regrowth which lowers the accuracy of burned area detection with multispectral imagery.
- **Cloud coverage**: Even if multispectral scenes were selected for low cloud coverage, there are still areas covered by clouds or cloud shadows which do not allow an extensive burned area detection.
- **Agricultural areas**: Especially agricultural fields are very dynamic as they are being harvested and prepared for new cultivation and considering the time difference between SAR and multispectral image acquisitions, there might be differences and also misclassifications in burned area classifications.

5.2 Emission estimation

The differences in fire emission estimations based on different datasets for carbon stock estimation are mostly due to the different land cover differentiation. ESA CCI land cover is a global product and the land cover classes are therefore coarser than in the MoEF land cover classification which is a national product and contains a finer class hierarchy. Figure 12 visualizes the relation between the different land cover categories of the two datasets. The MoEF classification differentiates 22 classes for Indonesia whereas the CCI land cover product distinguishes 16 land cover classes. However, for this figure only 9 out of these 16 land cover classes were selected for the CCI land cover product because the others covered only marginal fractions. It is clearly visible that the land cover class definitions differ substantially. The CCI land cover class *"Tree cover, broadleaved, evergreen, closed to open (>15%)"* is for example built up by roughly 90% by these MoEF classes: "*Primary Dry Land Forest*", *"Secondary Dry Land Forest"*, *"Primary Swamp Forest"*, *"Scrubland"*, *"Secondary Swamp Forest"*, *"Swamp Scrubland"*, *"Dry Rice Land"*, *"Dry Rice Land Mixed w/Scrub"*. These differences have direct impact on the vegetation emission estimations and hence the applied peat emission calculations (see ATBD [4]).

Moreover, this fact is also emphasized in the emission estimation comparison inside the 100,000 km² reference site based on the reference, MoEF and CCI land cover, respectively. Figure 13 depicts how diverse the detailed landscape in some areas is, which is neither represented in the CCI nor in the MoEF land cover classification but in the reference map. It also depicts a LiDAR transect in this area with

according aboveground biomass (AGB) values which supports the previous statement about the diverse landscape. Furthermore, the CCI land cover classification has a spatial resolution of 300 m which does not allow to differentiate such detailed patterns as depicted in Figure 13. This is very similar for the MoEF classification, even though it is based on Landsat and has therefore a spatial resolution of 30 m. The reference map on the other hand shows the different land cover classes at a very high spatial detail. The reference land cover map was created for this 100,000 km^2 reference site whereas the MoEF classification was created for a national scale and the CCI land cover map even for a global scale which is very clearly visible in the details of the respective classifications. In addition, it is also difficult to compare the resulted fire emissions due to the different mapping dates. The CCI land cover classification is based on the year 2010 (from 2008 to 2012), the MoEF classification is based on 2013 and the reference map is based on the pre-fire LC conditions of 2015.

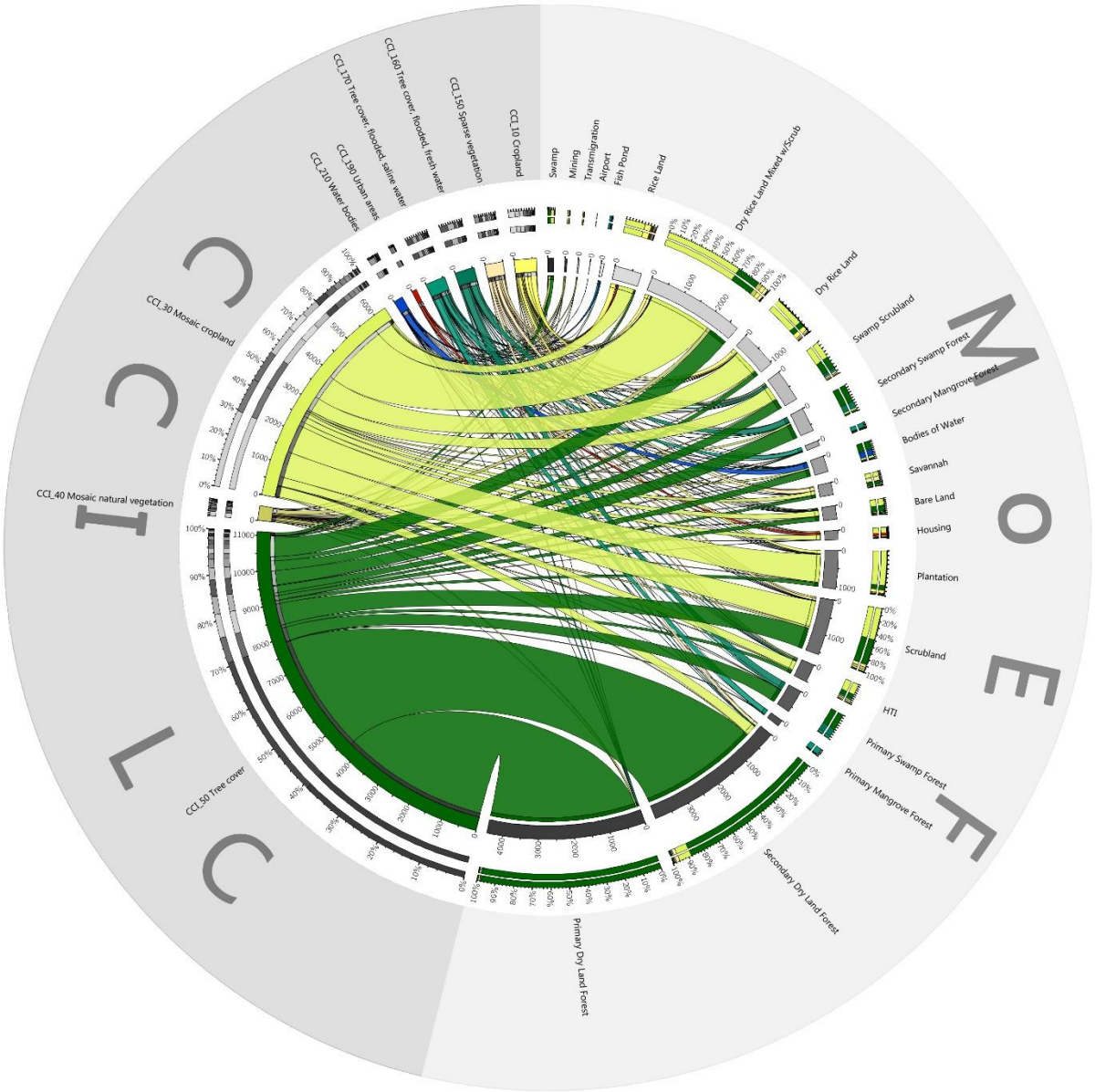

Figure 12: Relation between the land cover classes of ESA CCI land cover of 2010 (left) and MoEF land cover of 2013 (right) for whole Indonesia.

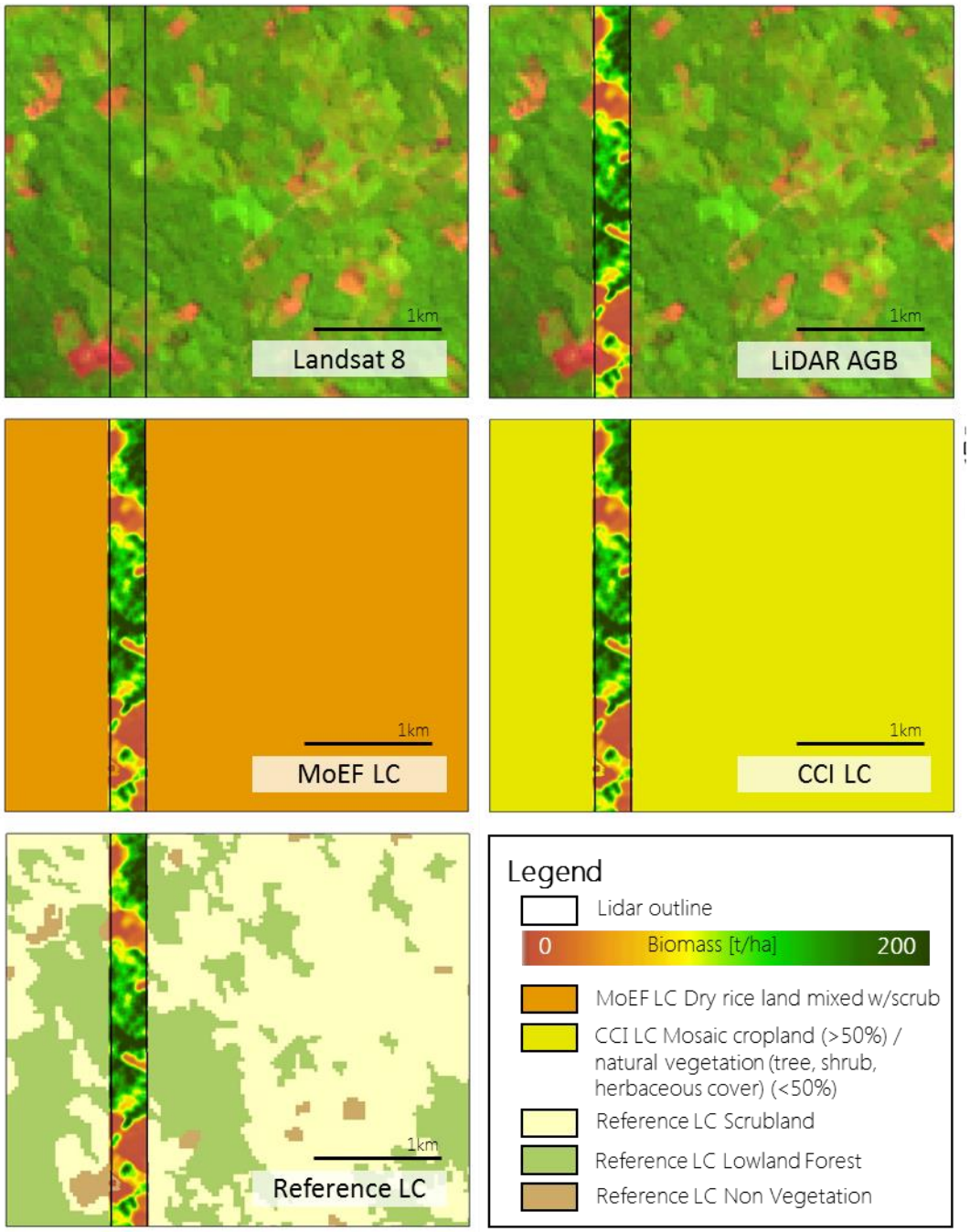

Figure 13: Comparison between Landsat image (top left), Landsat image superimposed by LiDAR AGB estimates (top right), LiDAR AGB estimates superimposed on MoEF LC (centre left), LiDAR AGB estimates with CCI land cover map (centre right) and LiDAR AGB estimates with the reference land cover classification.

The global fire emission database (GFED) [1] estimates Indonesia's fire emission from 2015 at 1,748 Mt CO_2-eq which is almost double than the emissions derived from our approach based on MoEF land cover map. The main difference between these two emission estimation approaches is the assumption of the mean peat burn depth. GFED assumes a mean peat burn depth of 30 cm for Indonesia [9] which is very similar to the results from a large-scale assessment of depth of burning in Borneo using LIDAR measurements [10]. More recent large-scale LiDAR studies on peat burn depth on Borneo suggest a discrimination between the first and second or more fires with regard to the burn depth into the peat and the amount of carbon released [11]. Following this study, a peat burn depth of 17 cm for the first

fire, and an average burn depth for the second and third fire, 8 cm, was used for two or more fires. Due to these lower numbers of average peat burn depth, our fire emission estimations are much lower than the ones from GFED. If we also assume a mean peat burn depth of 30 cm without any discrimination on the number of fire events, our fire emission estimate would be around 1,735 Mt CO_2-eq using Sentinel-1 burned areas and MoEF land cover map which is very similar to the GFED estimation. Known sources of uncertainty in the GFED fire emission estimation are a possible underestimation of burned area due to cloud and smoke cover [12].

5.3 PALSAR-2 cross comparison

The precipitation maps in Figure 14 show the precipitation during and three days before the image acquisitions of PALSAR-2 and Sentinel-1, respectively. In both pre-fire acquisitions light rain is visible in the study area (black rectangle). In the post-fire acquisitions there was less precipitation during and before the PALSAR-2 acquisition on 21/10/2015 and significantly more for the Sentinel-1 post-fire acquisition. Precipitation highly influences the backscatter of SAR and therefore needs to be taken into account when comparing datasets or their products.

Besides the precipitation influence, the difference of backscatter signal change after a fire event can be explained by the different polarizations. Horizontal polarized waves lead to a so called "double bounce" effects in fresh burned areas which increases the backscatter signal. This is the case for PASLAR-2. Having vertically polarized waves, as Sentinel-1, this effect is not obvious. Additionally, the change of backscatter in lower biomass ranges (scrub, grassland etc.) is better captured in the C-band SAR data of Sentinel-1 due to shorter wavelengths. This interpretation helps to understand the different spatial extension of classified burned areas using PALSAR-2 and Sentinel-1.

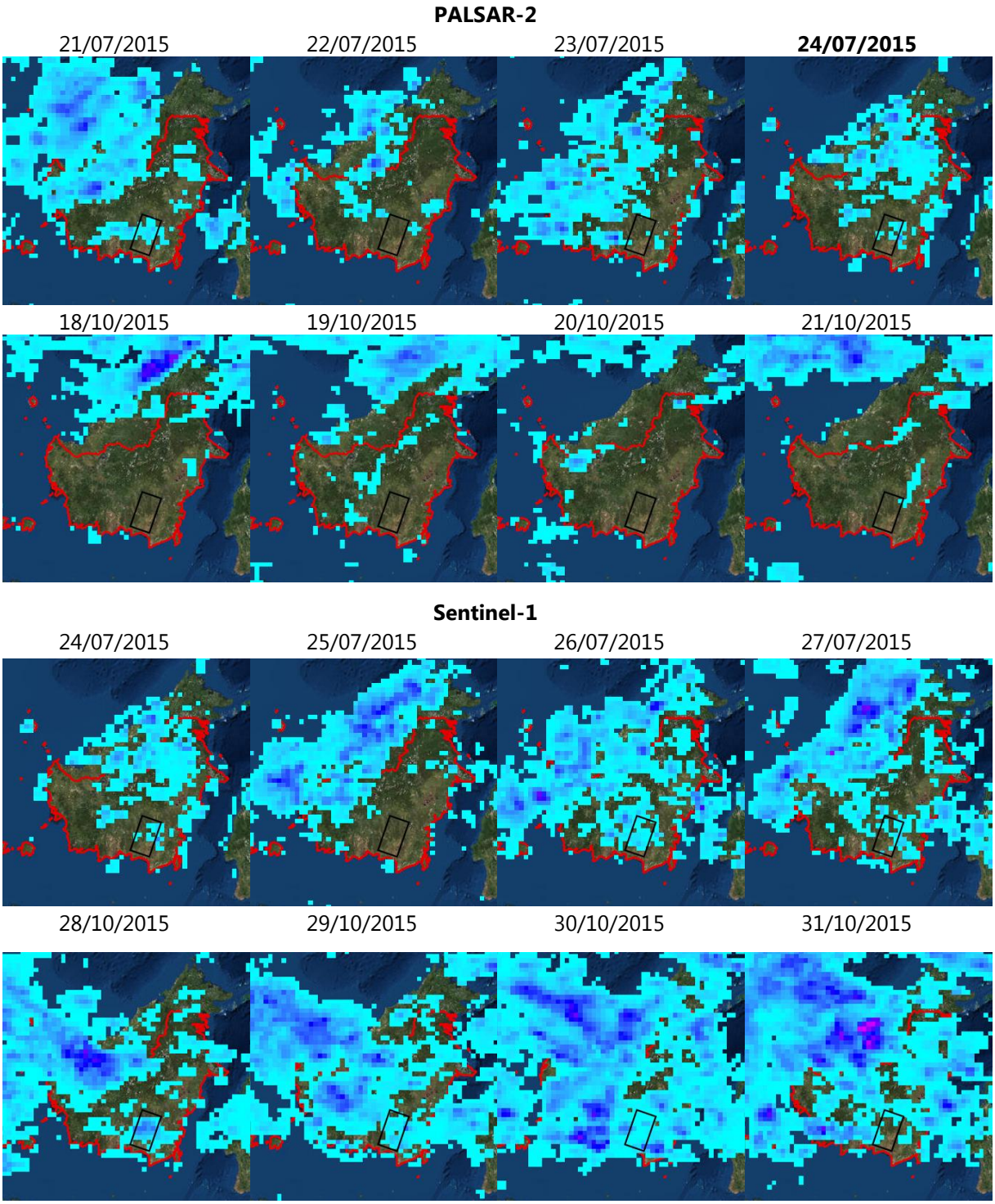

Figure 14: Precipitation (TRMM) before and during the PALSAR-2 and Sentinel-1 image acquisitions.

6 References

[1] GFED, "Global Fire Emission Database," 2015. [Online]. Available: http://www.globalfiredata.org/updates.html.

[2] L. Giglio, J. Descloitres, C. O. Justice, and Y. J. Kaufman, "An Enhanced Contextual Fire Detection Algorithm for MODIS," *Remote Sens. Environ.*, vol. 87, no. 2–3, pp. 273–282, Oct. 2003.

[3] A. E. Melchiori, A. W. Setzer, F. Morelli, R. Libonati, P. de A. Cândido, and S. C. de Jesús, "A Landsat-TM/OLI algorithm for burned areas in the Brazilian Cerrado: preliminary results," in *Advances in forest fire research.*, Coimbra, 2014, p. 30.

[4] S. Lohberger, M. Stängel, and F. Siegert, "D1 Algorithm Theoretical Basis Document." ESA CCI ECV Fire Disturbance, https://www.esa-fire-cci.org/, 2016.

[5] T. M. Lillesand, R. W. Kiefer, and J. W. Chipman, "Remote sensing and image interpretation.," no. Ed.5, 2008.

[6] R. G. Congalton and K. Green, *Assessing the Accuracy of Remotely Sensed Data: Principles and Practices, Second Edition (Google eBook)*. 2008.

[7] S. Baier, "Brandflächenklassifizierung in Riau, Sumatra, unter Verwendung mittelauflösender Fernerkundungsdaten," Paris Lodron-Universität Salzburg, 2014.

[8] M. Padilla, E. Chuvieco, S. Hantson, R. Theis, and C. Sandow, "D2.1-Product Validation Plan." ESA CCI ECV Fire Disturbance, https://www.esa-fire-cci.org/webfm_send/241, 2011.

[9] G. R. van der Werf, J. T. Randerson, L. Giglio, G. J. Collatz, M. Mu, P. S. Kasibhatla, D. C. Morton, R. S. DeFries, Y. Jin, and T. T. van Leeuwen, "Global fire emissions and the contribution of deforestation, savanna, forest, agricultural, and peat fires (1997–2009)," *Atmos. Chem. Phys.*, vol. 10, no. 23, pp. 11707–11735, Dec. 2010.

[10] U. Ballhorn, F. Siegert, M. Mason, and S. Limin, "Derivation of burn scar depths and estimation of carbon emissions with LIDAR in Indonesian peatlands," *Proc. Natl. Acad. Sci. U. S. A.*, vol. 106, no. 50, pp. 21213–21218, 2009.

[11] K. Konecny, U. Ballhorn, P. Navratil, J. Jubanski, S. E. Page, K. Tansey, A. Hooijer, R. Vernimmen, and F. Siegert, "Variable carbon losses from recurrent fires in drained tropical peatlands.," *Glob. Chang. Biol.*, Dec. 2015.

[12] L. Giglio, J. T. Randerson, and G. R. van der Werf, "Analysis of daily, monthly, and annual burned area using the fourth-generation global fire emissions database (GFED4)," *J. Geophys. Res. Biogeosciences*, vol. 118, no. 1, pp. 317–328, Mar. 2013.